

# Simultaneous Imaging of Endogenous Survivin mRNA and On-Demand Drug Release in Live Cells by Using a Mesoporous Silica Nanoquencher

Peiyan Yuan, Xin Mao, Kok Chan Chong, Jiaqi Fu, Sijun Pan, Shuizhu Wu, Changmin Yu,\* and Shao Q. Yao\*

*The design of multifunctional drug delivery systems capable of simultaneous target detection, imaging, and therapeutics in live mammalian cells is critical for biomedical research. In this study, by using mesoporous silica nanoparticles (MSNs) chemically modified with a small-molecule dark quencher, followed by sequential drug encapsulation, MSN capping with a dye-labeled antisense oligonucleotide, and bioorthogonal surface modification with cell-penetrating poly(disulfide)s, the authors have successfully developed the first mesoporous silica nanoquencher (qMSN), characterized by high drug-loading and endocytosis-independent cell uptake, which is able to quantitatively image endogenous survivin mRNA and release the loaded drug in a manner that depends on the survivin expression level in tumor cells. The authors further show that this novel drug delivery system may be used to minimize potential cytotoxicity encountered by many existing small-molecule drugs in cancer therapy.*

## 1. Introduction

In recent years, nanotechnology has attracted much attention in biomedical research. Among various nanomaterials, mesoporous silica nanoparticles (MSNs) are widely used in drug delivery and diagnostics/bioimaging.<sup>[1]</sup> These organosilicon materials could be readily prepared in the typical range of 50–200 nm to possess periodic pores of several nanometers, capable of efficiently encapsulating a variety of

cargos.<sup>[2]</sup> In addition to key properties such as high cargo loading capacity, good biocompatibility, and easy surface functionalization, the inert architectures of these nanomaterials further endow the encapsulated cargo with good intracellular stability. By choices of different gatekeepers to cap the surface of cargo-loaded nanoparticles, MSNs may facilitate delivery and controlled release of drugs exclusively to the intended cells and tissues, without provoking adverse side effects commonly associated with small-molecule drugs.<sup>[3]</sup> To date, numerous types of “gated” MSNs have been reported.<sup>[4]</sup> Among them, nucleic acid capped MSNs are highly attractive as they offer a sequence-encoded universal strategy of drug release that may be triggered by any endogenous DNAs/RNAs expressed in tumor cells or tissues.<sup>[5]</sup> By using chemically modified antisense oligonucleotide (ASO)-capped MSNs, we recently reported a drug delivery system capable of intracellular controlled release of drugs in a manner dependent upon the endogenous expression of microRNAs (i.e., well-known small noncoding regulatory RNAs).<sup>[6]</sup> Whether or not a similarly gated system can effect such on-demand drug release by other endogenous genetic materials (i.e., mRNAs) is, however, unknown. Furthermore, the

Dr. P. Yuan, X. Mao, K. C. Chong, Dr. J. Fu, S. Pan,  
Prof. S. Q. Yao  
Department of Chemistry  
National University of Singapore  
3 Science Drive 3, 117543 Singapore, Singapore  
E-mail: chmyaosq@nus.edu.sg

Prof. S. Wu, Dr. C. Yu  
College of Materials Science and Engineering  
South China University of Technology  
510640 Guangzhou, China  
E-mail: yucm@scut.edu.cn



DOI: 10.1002/sml.201700569

cellular uptake of these nanoparticles was facilitated by covalent modification of the MSN surface with cell-penetrating peptides, which caused severe endolysosomal trapping and led to slow/poor cytosolic release of MSNs.<sup>[7]</sup> Such problems are even more pronounced with larger-size MSNs (>100 nm) which are needed to ensure high drug-loading capacity.<sup>[1,2]</sup> It was found that prolonged incubations with cells were needed in order to achieve sufficient intracellular uncapping of such MSNs (>6 h) and their subsequent drug release (12–24 h).<sup>[6,8]</sup> Such a time scale is clearly unacceptable if the MSNs are intended for theranostic applications to image the target, drug release, and/or the drugs biological effects.<sup>[8]</sup>

Nucleic-acid-based reagents capable of mRNA imaging and quantification are widely available, but a few are able to enter mammalian cells on their own, and thus offer limited utilities for intracellular applications.<sup>[9]</sup> Recent advances in nanotechnology have fueled the development of gold nanoparticle (AuNP)-coupled fluorescent DNA probes, which are suitable for real-time and quantitative imaging of endogenous mRNAs.<sup>[10]</sup> The many favorable properties that these AuNPs possess, including cell permeability (albeit mostly with endocytosis uptake mechanism),<sup>[10a]</sup> strong nucleic-acid-binding, resistance to degradation, and distance-dependent fluorescence quenching, make them well-suited for the design of various fluorescence Turn-ON nanosensors capable of responding to different endogenous biomolecules and/or stimuli.<sup>[11]</sup> One major shortcoming of existing AuNP-based mRNA nanosensors lies in their limited intracellular detection sensitivity, which stems from the intrinsically low probe-loading capacity due to small nanoparticle sizes ( $\leq 10$  nm), as well as slow/poor cytosolic release due to endocytosis.<sup>[10,12]</sup> Introduction of enzyme-free signal amplification techniques, such as hybridization chain reaction into these nanosensors, has presumably led to the improved detection limit.<sup>[13a]</sup> Another major problem with AuNP-based mRNA biosensors is their limited ability to be doubled as effective drug delivery systems, unlike MSNs.<sup>[10b]</sup> Consequently, theranostic nanoparticles capable of both quantitative imaging of endogenous mRNAs and efficient drug delivery (and on-demand release) are, to our knowledge, unavailable at present.<sup>[14]</sup>

Herein, we report the successful development of new theranostic MSNs that achieved not only intracellular controlled release of an encapsulated drug in a manner dependent upon the endogenous expression level of a target mRNA, but also quantitative imaging of both the target (i.e., mRNA) and the drug release process (**Scheme 1**). It may also be used to minimize potential cytotoxicity encountered by many existing small molecule drugs in cancer therapy.<sup>[3]</sup> The ability to image endogenous mRNAs in live mammalian cells and tissues is important in revealing the expression, localization, and dynamics of these essential cellular molecules.<sup>[15]</sup>

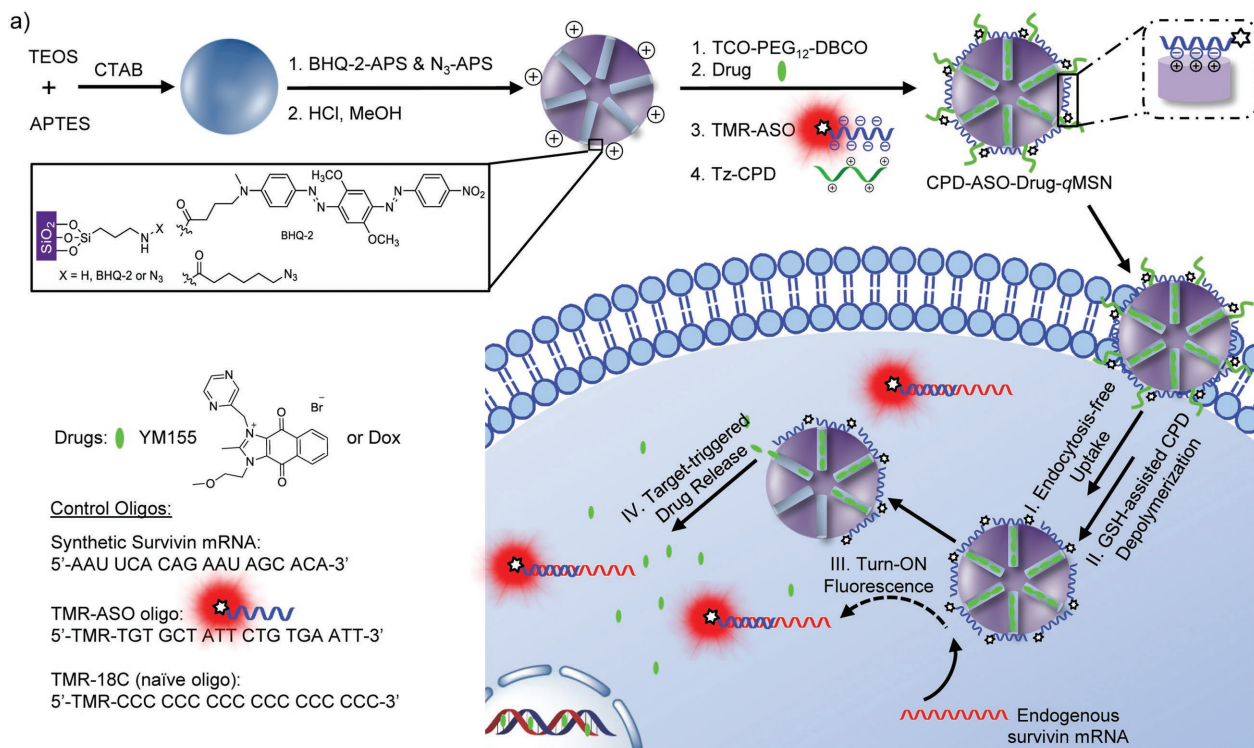
## 2. Results and Discussion

Overall strategy of our newly developed theranostic MSNs is shown in Scheme 1. A key feature of these multifunction MSNs for simultaneous imaging of endogenous mRNAs and on-demand drug release was the use of a mesoporous silica

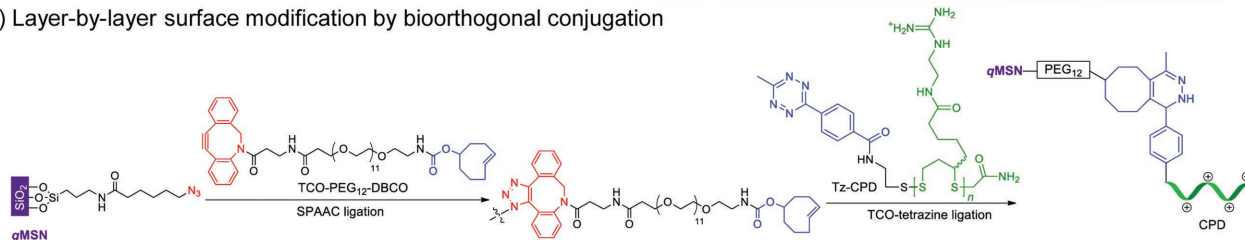
nanoquencher (*q*MSN), obtained by conjugating a small-molecule fluorescence dark quencher (Black Hole Quencher (BHQ), BHQ-2) to amine-functionalized MSNs (MSN-NH<sub>2</sub>). BHQ-2 was chosen because its absorption spectrum (550–650 nm) overlaps well with the emission spectrum of tetramethylrhodamine (TMR). Similar BHQ-2-modified nanoquenchers were previously reported as fluorescent sensors to detect endogenous enzymatic activities,<sup>[16]</sup> but never as dual-imaging drug delivery systems. By optimizing the amount of BHQ-2 modified on the surface of positively charged nanoparticles, followed by drug encapsulation and capping with a negatively charged TMR-labeled ASO (via electrostatic interaction), we successfully synthesized ASO-Drug-*q*MSN that possessed both good fluorescence quenching efficiency (QE) ( $\approx 94\%$ ) and high drug-loading capacity ( $>58$  mol g<sup>-1</sup> for Doxorubicin, or Dox). Typical AuNPs and MSNs would possess one of these two properties, respectively; but not both.<sup>[1,2,10]</sup> Deviated from our previous work, in which chemically modified ASO was used both as a gatekeeper and a microRNA inhibitor by antisense technology,<sup>[6]</sup> the survivin ASO used in the current work (Scheme 1a), with the exception of TMR labeling, was not chemically modified, and therefore was capable of binding to survivin mRNA via sequence complementarity, but not affecting its endogenous expression level.<sup>[17]</sup> Survivin is an important tumor biomarker that promotes cell proliferation, and high levels of survivin (at both mRNA and protein levels) are found in most cancer cells.<sup>[18]</sup>

Another important feature of above *q*MSN was that, after ASO capping, an additional coating of cell-penetrating poly(disulfide)s (CPD) was introduced to the outermost layer of the nanoparticles (giving CPD-ASO-Drug-*q*MSN). This was done by treatment of the *q*MSN surface with N<sub>3</sub>-APS (ammonium persulfate), followed by successive bio-orthogonal ligation with TCO-PEG<sub>12</sub>-DBCO and Tz-CPD (Scheme 1b).<sup>[19]</sup> We found this “layer-by-layer” surface modification was necessary to ensure the resulting nanoparticles entered the cytosol of mammalian cells via endocytosis-independent pathways (Step I) followed by glutathione (GSH)-assisted rapid depolymerization of CPD ( $<5$  min;<sup>[20]</sup> Step II), before being exposed to any endogenous survivin mRNA. Compared to other endocytic nanoparticles,<sup>[10]</sup> CPD-conjugated nanoparticles were previously shown to be rapidly and efficiently uptaken by mammalian cells without endolysosomal trapping,<sup>[21]</sup> and we were hopeful that this important quality would further boost the mRNA imaging capability of these *q*MSNs. Next, in the presence of cytosolic survivin mRNA, the *q*MSN-bound, fluorescently quenched TMR-ASO would undergo hybridization and get detached from the positively charged *q*MSN surface, resulting in an immediate and proportional release of fluorescence signals (Step III). Concurrently, the dissociation of TMR-ASO gatekeeper would also cause the uncapped *q*MSN to release the loaded drug intracellularly (Step IV).

Detailed synthesis of CPD-ASO-Drug-*q*MSN and control MSNs are provided in Figure S1 and S2 in the Supporting Information. The chemical, biochemical, and physical properties of these nanoparticles were characterized by transmission electron microscopy (TEM), Brunauer–Emmett–Teller (BET), Fourier transform infrared (FTIR), Zeta potential,



b) Layer-by-layer surface modification by bioorthogonal conjugation



**Scheme 1.** a) Overall strategy for the preparation of CPD-ASO-Drug-qMSN and subsequent cellular uptake via endocytosis-independent pathways (I), GSH-assisted CPD depolymerization (II), imaging of endogenous survivin mRNA (III), and on-demand release of drug (IV). b) Scheme showing the chemistries used for layer-by-layer surface qMSN modification with N<sub>3</sub>, SPAAC ligation between N<sub>3</sub> and DBCO of TCO-PEG<sub>12</sub>-DBCO, and finally TCO-tetrazine ligation between TCO and the tetrazine of Tz-CPD.

and other measurements as previously described (**Figure 1** and Figure S3, Supporting Information).<sup>[6]</sup> Briefly, highly monodispersed MSN-NH<sub>2</sub> was first prepared (mean size: 120.7 ± 6.4 nm) and possessed a uniform pore size of 2.6 nm. Subsequently, as-synthesized BHQ-2-APS was introduced as previously reported.<sup>[16]</sup> We optimized the amount of BHQ-2 modified on MSNs to obtain high quenching efficiency for TMR-ASO after capping, and a 94% quenching efficiency was achieved with an estimated 10.67 μmol g<sup>-1</sup> of BHQ-2 loading, as shown in Figure S4 in the Supporting Information. The amount of capping TMR-ASO was determined by fluorescence measurement to be 18.46 μmol g<sup>-1</sup>, and the corresponding controlled release experiments were similarly done in the presence of synthetic survivin mRNA under in vitro conditions (**Figure 2a**); while an ASO-qMSN solution displayed very weak fluorescence, its fluorescence intensity increased proportionally upon addition of synthetic survivin mRNA, indicating successful detachment of TMR-ASO from the qMSN surface as a result of sequence-matched recognition by the synthetic survivin mRNA. We observed a 5.2-fold Turn-ON fluorescence of ASO-qMSN in

the presence of 2 × 10<sup>-6</sup> M of synthetic survivin mRNA and a calculated detection limit of 1.3 × 10<sup>-9</sup> M, with a linear correlation at λ<sub>em</sub> = 580 nm in the range of 0 to 100 × 10<sup>-9</sup> M (inset in Figure 2b). As shown in **Figure 3a**, while most of TMR fluorescence from detached TMR-ASO of the nanosensor upon addition of synthetic survivin mRNA could be recovered in <2 h, no obvious fluorescence increase was observed with a non-complimentary mRNA (control 18A RNA), even after prolonged incubation (24 h; Figure 3a). Similar fluorescence Turn-ON profiles were obtained with ASO-qMSN incubated with different amounts of total RNA isolates of HeLa cells, which are known to have elevated endogenous survivin mRNA expression (Figure S5a, Supporting Information).<sup>[13]</sup> These results indicate our newly developed nanosensor has the potential to sensitively and quantitatively detect and image endogenous survivin mRNA in a sequence-specific manner with relatively short response time.

Next, the intrinsically fluorescent Dox (an anticancer drug) was loaded into ASO-qMSN to monitor the controlled release process of the drug in response to survivin mRNA. The amount of loaded Dox as well as its subsequent

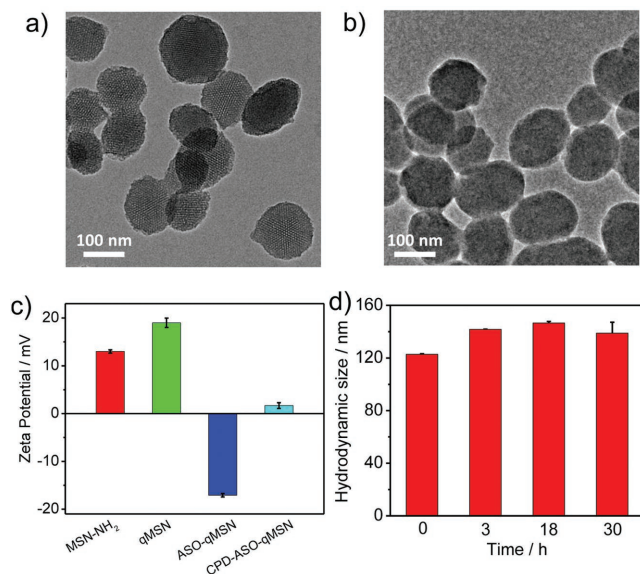


**Figure 1.** TEM image of a) MSN-NH<sub>2</sub> without CTAB and b) ASO-qMSN without CTAB. c) Zeta potentials of different MSNs. d) DLS size measurements of CPD-ASO-qMSN incubated in DMEM medium for different periods of time (0, 3, 18, 30 h).

release from the resulting ASO-Dox-qMSN was quantitatively determined by fluorescence measurements of Dox (Figure 3 and Figures S4 and S5, Supporting Information), and the Dox loading capacity was determined to be 58.85  $\mu\text{mol g}^{-1}$  (Figure S4d, Supporting Information). Time-dependent Dox release from ASO-Dox-qMSN was observed in the presence of  $0.3\text{--}2.0 \times 10^{-6}$  M of synthetic survivin mRNA, which showed >80% Dox was successfully released after 24 h incubation (at 37 °C), while <10% of drug leakage was detected during the same period with either a “wrong” mRNA (e.g.,  $2.0 \times 10^{-6}$  M of 18A RNA) or no mRNA. Longer incubation and increasing amounts of synthetic survivin mRNA both led to proportional increases of Dox release (Figure 3b), indicating this “smart” drug delivery system would enable dose-dependent, controlled release of a small molecule drug in tumor cells in response to important endogenous tumor biomarkers such as survivin mRNA. A linear relationship between the amount of Dox release ( $x$ -axis) and the fluorescence intensity ( $y$ -axis) from the detached TMR upon addition of different doses of synthetic survivin mRNA and different incubation time further showed (Figure 3c,d), while our qMSN was designed to image endogenous survivin mRNA, the TMR fluorescence from such experiments could also be used to quantitatively monitor the relative amount of the encapsulated drug released from the nanoparticles, including those without intrinsic fluorescence. Finally, the biochemical stability of ASO-Dox-qMSN in cellular environments was tested in a model experiment by treating the nanoparticles with DNAase I (up to 5 U mL<sup>-1</sup>)

for 24 h (Figure S3e,f, Supporting Information); fluorescence increases from either TMR or Dox channel (indicator of possible TMR-ASO degradation or premature Dox release, respectively) was not observed, thus confirming that, in our subsequent live-cell experiments, successful fluorescence Turn-ON and ensuing drug release were caused by endogenous target recognition and not serendipitous nuclease degradation of the TMR-ASO gatekeeper. Previously, it was observed that the high-affinity electrostatic assembly of DNA on the cationic surface of MSNs probably cause high steric hindrance for nuclease to interact with DNA, thus effectively protecting DNA against potential degradation.<sup>[6,13]</sup>

We next determined the endogenous mRNA imaging property of these nanoparticles in live mammalian cells. An additional coating of CPD was introduced to TMR-ASO-capped qMSN, as earlier described, giving CPD-ASO-qMSN (no drug) and CPD-ASO-Drug-qMSN (with a drug). The resulting nanoparticles showed negligible aggregation in Dulbecco’s Modified Eagle Medium (DMEM) after 30 h incubation (Figure 1d). Cellular uptake and survivin mRNA imaging capability of CPD-ASO-qMSN in HeLa cells were next examined by using confocal laser scanning microscopy (CLSM). In order to confirm the endocytosis-independent cell uptake of CPD modified MSNs, detailed uptake studies were conducted by using FITC-labeled MSNs as model cargos (Figure S6, Supporting Information). Unlike control MSNs without CPD modification (FITC-MSN-NH<sub>2</sub>), cell uptake of CPD-FITC-MSN was not sensitive to treatment by most endocytosis inhibitors. Treatment of cells with a thiol-mediated translocation inhibitor, 5,5’-dithiobis-2-nitrobenzoic acid, on the other hand, caused significant inhibition of CPD-FITC-MSN uptake. Moreover, no significant endolysosomal trapping was observed when CPD-FITC-MSN entered cells. Such results are consistent with our previous studies,<sup>[21]</sup> and again confirm the endocytosis-independent, thiol-mediated cell uptake mechanism of CPD-modified MSNs.<sup>[20]</sup> After that, RGD-ASO-qMSN, which were prepared by capping qMSN with TMR-ASO followed by coating with an arginylglycylaspartic acid (RGD) peptide and were expected

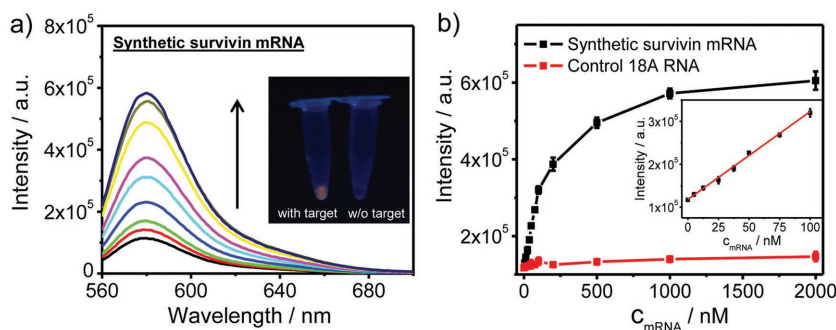


**Figure 2.** a) Fluorescence spectra ( $\lambda_{\text{ex}} = 545$  nm) of ASO-qMSN (0.1 mg mL<sup>-1</sup> in PBS) incubated with varying concentrations of synthetic survivin mRNA (0  $\times 10^{-9}$  M, 12.5  $\times 10^{-9}$  M, 25  $\times 10^{-9}$  M, 50  $\times 10^{-9}$  M, 100  $\times 10^{-9}$  M, 200  $\times 10^{-9}$  M, 500  $\times 10^{-9}$  M, 1000  $\times 10^{-9}$  M, 2000  $\times 10^{-9}$  M) at 37 °C for 2 h. Inset: Photos of the ASO-qMSN sample (boxed in Figure S4b, Supporting Information) taken under UV ( $\lambda_{\text{ex}} = 365$  nm), after incubation with (left) or without (right) synthetic survivin mRNA. b) Plot of fluorescence intensity of ASO-qMSN (0.1 mg mL<sup>-1</sup> in PBS; 37 °C for 2 h) versus target concentrations (synthetic survivin mRNA: black; control 18A RNA: red). Inset: plot of fluorescence intensity ( $\lambda_{\text{em}} = 580$  nm) of ASO-qMSN versus synthetic survivin mRNA (0 to 100  $\times 10^{-9}$  M).

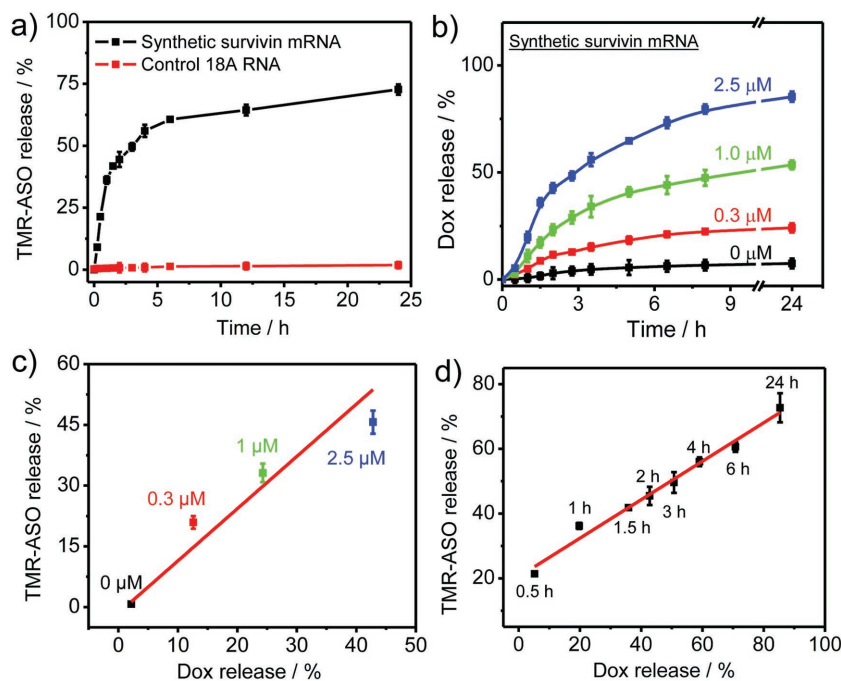


**Figure 3.** a) Time-dependent fluorescence increase of ASO-*q*MSN ( $0.1 \text{ mg mL}^{-1}$  in PBS at  $37^\circ\text{C}$ ,  $\lambda_{\text{em}} = 580 \text{ nm}$ ) upon addition of different targets (target concentrations:  $2.5 \times 10^{-6} \text{ M}$ , synthetic survivin mRNA: black; control 18A RNA: red). b) Time-dependent Dox release from ASO-Dox-*q*MSN ( $0.1 \text{ mg mL}^{-1}$  in PBS at  $37^\circ\text{C}$ ) upon incubation with synthetic survivin mRNA ( $0, 0.3, 1.0, 2.5 \times 10^{-6} \text{ M}$ ). c) Plot of fluorescence intensity ( $\lambda_{\text{em}} = 580 \text{ nm}$ ) of ASO-*q*MSN versus % Dox release ( $\lambda_{\text{ex}} = 488 \text{ nm}$ ,  $\lambda_{\text{em}} = 558 \text{ nm}$ ) after 2 h incubation (at  $37^\circ\text{C}$ ) with different amounts of synthetic survivin mRNA. d) Time-dependent plot of fluorescence intensity of released TMR-ASO versus released Dox after ASO-Dox-*q*MSN ( $0.1 \text{ mg mL}^{-1}$  in PBS) was incubated with  $2.5 \times 10^{-6} \text{ M}$  of synthetic survivin mRNA.

to be uptaken by mammalian cells via endocytosis,<sup>[6]</sup> were used as another type of control nanoparticles to confirm our earlier hypothesis, that is, the rapid, efficient, and endocytosis-independent cell uptake properties expected from CPD-ASO-*q*MSN would render them more superior for live-cell quantitative imaging of endogenous survivin mRNA than traditional endocytic nanosensors.<sup>[10a]</sup> CPD-18C-*q*MSN, prepared by capping *q*MSN with TMR-18C (a naive gatekeeper; Scheme 1a) followed by CPD coating, were designed to validate that, only a properly gated nanosensor (i.e., CPD-ASO-*q*MSN) would enable successful imaging of endogenous survivin mRNA. CLSM of live HeLa cells treated with CPD-ASO-*q*MSN showed visible TMR fluorescence in as little as 20 min of individual cells (Figure 4a), indicating successful cell uptake of the nanosensor and subsequent target recognition/TMR-ASO release. The TMR fluorescence signals continued to increase over the course of 4 h, as more nanosensors reached the cytosol where endogenous survivin mRNA resided, resulting in the release of free TMR-ASO, which led to a further increase in TMR fluorescence. Side-by-side comparison of HeLa cells treated with control nanoparticles showed even more pronounced differences in their single-cell mRNA imaging capability (Figure 4b, 4 h incubation); very strong TMR fluorescence was detected throughout the cytosol of CPD-ASO-*q*MSN-treated cells (top panels), while significantly weaker and no TMR fluorescence signals were detected in RGD-ASO-*q*MSN and

CPD-18C-*q*MSN treated cells (middle and bottom panels), respectively. All results were further quantified (Figure S7, Supporting Information) Next, we ascertained whether these nanosensors could be used to quantitatively image and differentiate survivin mRNA levels expressed in various mammalian cells. In addition to HeLa cells, which are known to have a high survivin expression,<sup>[13,18]</sup> MCF-7 cells (medium survivin expression) and MCF-10A cells (low/minimum survivin expression) were treated with CPD-ASO-*q*MSN and imaged (Figure 4c); strong, medium, and weak/no TMR fluorescence signals were detected in cytosols of the treated cells, and these imaging-based results correlated well with the relative expression levels of endogenous survivin mRNA concurrently determined by real-time quantitative PCR (*q*PCR; Figure S9, Supporting Information). These survivin mRNA-responsive TMR fluorescence changes were further quantified using the flow cytometry (Figure 4c, right). We further expanded this quantitative imaging-based survivin mRNA detection method to other mammalian cell lines (i.e., A549, A431, PC3, HepG2, HEK 293T). Instead of quantifying survivin mRNA at single-cell level, which might not be as accurate due to cell-to-cell variations, we used an

imaging-based high-content screening (HCS) system to analyze a large pool of nanosensor-treated cells (Figure 4d and Figure S10 in the Supporting Information); a nearly linear relationship between *q*PCR results and average TMR signals obtained from the HCS experiment further confirmed our newly developed nanosensors could indeed be used to quantitatively image endogenous survivin mRNA at single-cell level or with an ensemble of cells at different spatial resolutions.

The on-demand drug release property of these *q*MSNs in response to endogenous survivin mRNA was next assessed. Previously reported survivin mRNA nanosensors do not have such drug-delivery capability.<sup>[10,13]</sup> Two recently developed MSNs only responded to microRNA or endogenous GSH and did not have any mRNA imaging capability.<sup>[6,21]</sup> As shown in Figure 4e,f, CPD-ASO-Dox-*q*MSN was used to treat HeLa cells, followed by time-dependent live-cell imaging under both TMR (red) and Dox channels (green); by simultaneously imaging both the endogenous survivin mRNA (TMR channel) and on-demand Dox release (Dox channel), we were able to closely monitor the sequential uncapping of TMR-ASO and release of encapsulated Dox from the *q*MSN. Similar to earlier observations (Figure 4a and Figure S8, Supporting Information), TMR fluorescence started to develop in 20 min, at which point no obvious Dox fluorescence was detected. At 40 min, the Dox fluorescence appeared, indicating a successful drug release. Further incubation led to

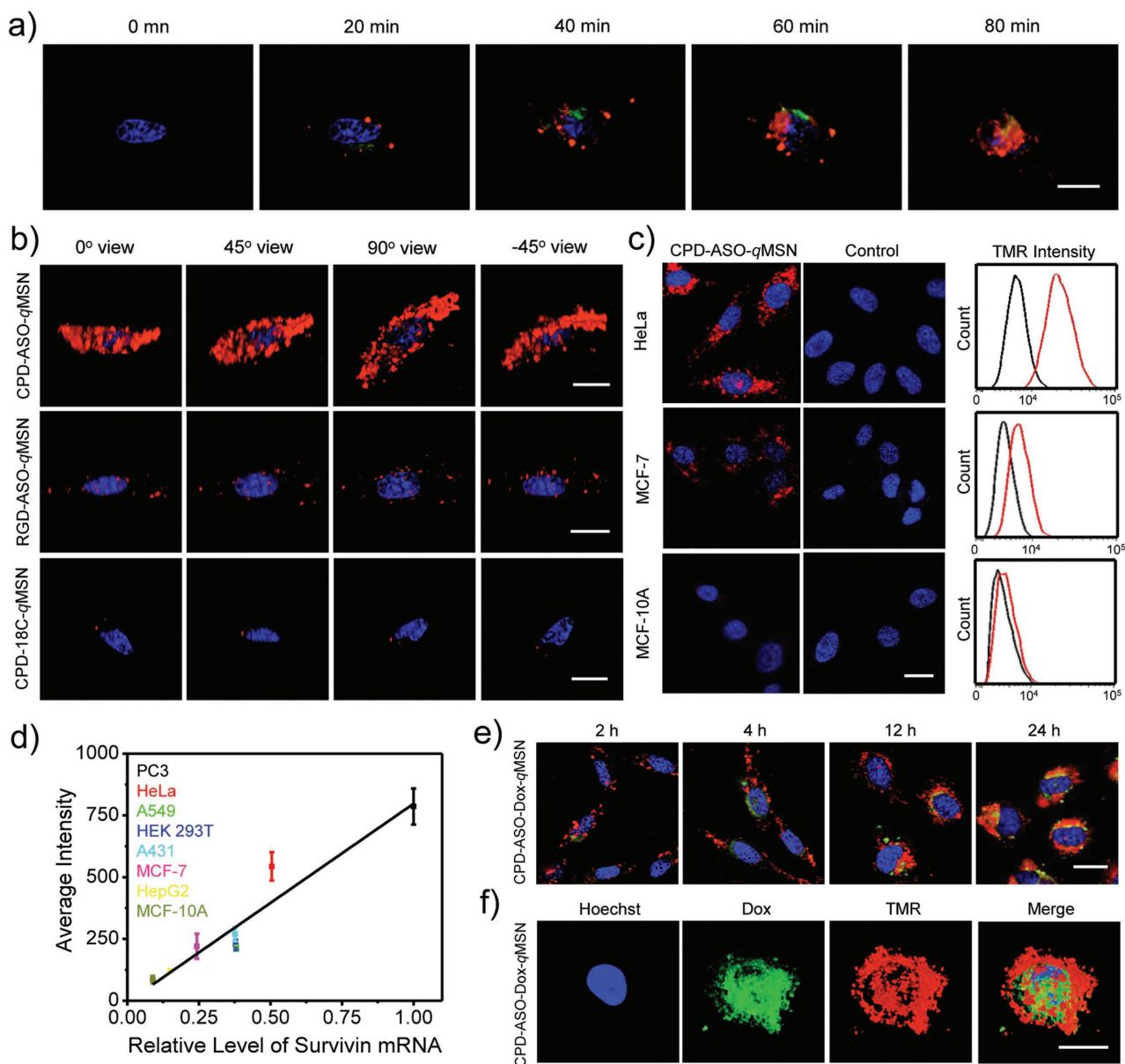


**Figure 4.** a) Real-time 3D projections of z-stack images at 90° view angles (step size = 0.163  $\mu\text{m}$ ) of live HeLa cells incubated with 10  $\mu\text{g mL}^{-1}$  CPD-ASO-Dox-qMSN for different lengths of time before image acquisition (0, 20, 40, 60, and 80 min). (Dox): green; (TMR): red; (Hoechst): blue. b) 3D projections of z-stack images at different view angles (0°, 45°, 90°, -45°) of HeLa cells treated with CPD-ASO-qMSN, RGD-ASO-qMSN and CPD-18C-qMSN (10  $\mu\text{g mL}^{-1}$ ; 4 h). Cells were stained with Hoechst (in blue). Turn-ON fluorescence from the TMR channel was colored in red. c) CLSM images of different mammalian cells treated (left) with and (middle) without CPD-ASO-qMSN (10  $\mu\text{g mL}^{-1}$ ; 4 h). (right) Flow cytometric results of different mammalian cells treated with CPD-ASO-qMSN (red, 10  $\mu\text{g mL}^{-1}$ , for 4 h), cells without any qMSN treatments were used as control (black). (x-axis): relative TMR fluorescence; (y-axis): cell count. d) Fluorescence quantification in different cell lines by HCS versus their endogenous survivin mRNA expression levels determined by qPCR. Cells were incubated with CPD-ASO-qMSN (10  $\mu\text{g mL}^{-1}$ ; 4 h). Error bars were obtained by analysis of triplicate tests. e) CLSM images of HeLa cells treated with 10  $\mu\text{g mL}^{-1}$  CPD-ASO-Dox-qMSN after different incubation time (2, 4, 12, 24 h). f) 3D projections of z-stack images at 90° view (step size, 0.163  $\mu\text{m}$ ) of HeLa cells treated with CPD-ASO-Dox-qMSN (10  $\mu\text{g mL}^{-1}$ ; 24 h). Scale bar = 20  $\mu\text{m}$ .

concomitant increases in both TMR and Dox fluorescence as more TMR-ASO uncapping and drug release occurred. This process continued until at  $\approx 24$  h, when both TMR and Dox signals reached saturation. 3D projections of z-stack images of these treated cells clearly showed the subsequent nuclear localization of released Dox, while the TMR fluorescence signals remained mostly in the cytosol (Figure 4f and Figure S11, Supporting Information). We observed apparent rounding in the cells indicative of apoptosis, which was subsequently

confirmed by flow cytometry (Figure S12, Supporting Information). We noted this intracellular drug-release profile was similar to that of earlier in vitro results (Figure 3), and that TMR fluorescence was detected prior to Dox fluorescence clearly indicate the role of TMR-ASO as a gatekeeper in preventing premature leakage of Dox. As expected, neither TMR nor Dox fluorescence was detected in control cells treated with CPD-18C-Dox-qMSN over 24 h (Figure S13, Supporting Information). To further confirm that our delivery system was

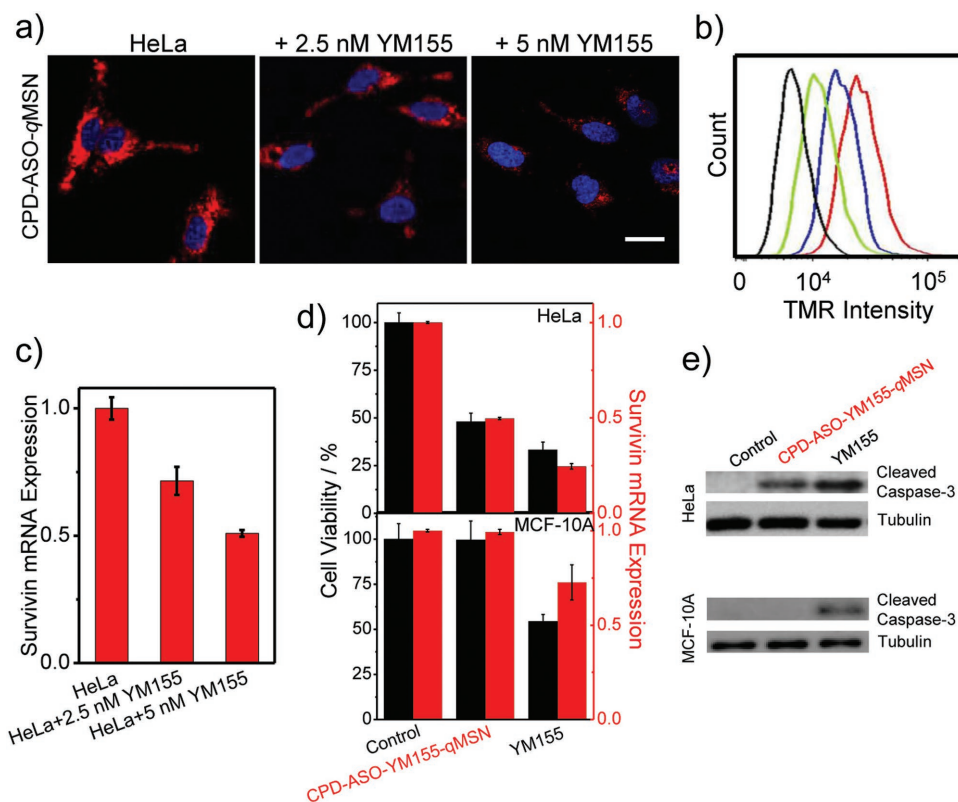


**Figure 5.** a) CLSM images of HeLa cells treated with YM155 ( $0 \times 10^{-9}$  M,  $2.5 \times 10^{-9}$  M,  $5 \times 10^{-9}$  M; 48 h) followed by mRNA imaging with CPD-ASO-*q*MSN ( $10 \mu\text{g mL}^{-1}$ ; 4 h). b) Flow cytometric results of HeLa cells treated with different amounts of YM155 ( $0 \times 10^{-9}$  M: red;  $2.5 \times 10^{-9}$  M: blue;  $5 \times 10^{-9}$  M: green) followed by incubation with CPD-ASO-*q*MSN ( $10 \mu\text{g mL}^{-1}$ , for 4 h). HeLa cells without any *q*MSN treatments were used as control (black). (x-axis): relative TMR fluorescence; (y-axis): cell count. c) *q*PCR determination of endogenous survivin mRNA expression from cells in (a). d) XTT cell viability test (black bars) and endogenous survivin mRNA expression levels (red bars) of HeLa (top graph) or MCF-10A (bottom graph) cells treated with different *q*MSNs ( $50 \mu\text{g mL}^{-1}$ ; 24 h). Control: DMSO-treated cells. Note: data in y-axis of each graph were normalized against “control” which was set as either 100% (cell viability) or 1 (survivin mRNA expression). e) WB analysis of cells in (d), with anti-cleaved caspase-3 and anti-tubulin (loading control), respectively. Scale bar = 20  $\mu\text{m}$ . Error bars were obtained by analysis of triplicate tests.

able to achieve survivin mRNA-responsive controlled drug release as well as quantitatively monitor the released amount of the encapsulated drug, cell lines with different survivin mRNA expression level were imaged after the treatment with CPD-ASO-Dox-*q*MSN (Figure S8c and S14, Supporting Information). Both TMR and Dox fluorescent signals correspondingly changed with the endogenous survivin mRNA level, indicating this new developed theranostic system can be utilized to simultaneously endogenous image both the target and drug release process.

Most small molecule drugs have side effects caused by off-targets and other issues. While advanced chemical tools have been developed that enable proteome-wide identification of potential cellular targets of bioactive compounds,<sup>[3,22–29]</sup> they do not make a drug less cytotoxic, unless new analogs are identified/tested. In order to side-step such off-target issues, we explored alternative “smart” drug delivery methods capable of delivering cytotoxic drugs to specific cells/tissues and releasing them at the right dosage. YM155 is an imidazolium-based compound that shows potent antitumor activities by effectively suppressing the endogenous survivin mRNA expression from a variety of cancer cells.<sup>[30,31]</sup> We wondered if our newly developed theranostic nanoparticles could be used to deliver YM155 into cancer cells, thus enabling both

target imaging and dose-dependent release of YM155 intracellularly with an auto-feedback inhibition mechanism, that is, the more endogenous survivin mRNA are detected in the nanoparticle-treated tumor cells, the more YM155 would be released to suppress its expression. As shown in **Figure 5a,b**, HeLa cells pretreated with different dosages of YM155 ( $0$ ,  $2.5$ ,  $5 \times 10^{-9}$  M for 48 h) followed by endogenous survivin mRNA imaging with CPD-ASO-*q*MSN clearly showed dose-dependent down-regulation of survivin mRNA with corresponding decreases in TMR fluorescence signals of treated cells, and these results were in good agreement with the *q*PCR data (Figure 5c and Figure S14, Supporting Information). Since most drugs including YM155 are not fluorescent and cannot be imaged directly, our earlier results showing a linear relationship between Turn-ON TMR signals and the relative amount of a released drug (Figure 3) mean that above-detected TMR signals also served as a reliable indicator to assess the relative amount of intracellularly released YM155 in the following experiments. First, YM155 was loaded into CPD-ASO-*q*MSN to give CPD-ASO-YM155-*q*MSN. Next, these drug-loaded nanoparticles were incubated with HeLa cells followed by XTT viability analysis (to measure cell killing effect), *q*PCR (to measure endogenous survivin mRNA expression), flow cytometry analysis and western

blotting (WB) analysis (to measure cell apoptosis). Control experiments with MCF-10A cells which have minimum survivin mRNA expression were concurrently carried out to assess whether CPD-ASO-YM155-*q*MSN was indeed able to minimize the cytotoxicity of YM155 by effectively killing ONLY survivin-overexpressing cancer cells, such as HeLa cells. As shown in Figure 5d,e and Figure S15, Supporting Information, while both cancer cells were effectively killed by free YM155 (indicative of the drug's intrinsic cytotoxicity), Only HeLa cells were killed by CPD-ASO-YM155-*q*MSN (top graph in Figure 5d; black bars); we observed >50% suppression of HeLa cell growth in the presence of these drug-loaded nanoparticles, while similarly treated MCF-10A cells showed negligible growth inhibition (bottom graph; black bars). The cell growth inhibition profiles corroborated well with corresponding changes in the survivin mRNA expression levels (red bars in Figure 5d), therefore unequivocally confirming our delivery system and its controlled drug release were indeed survivin mRNA-responsive. Finally, WB analysis further confirmed that, only YM155-loaded nanoparticles capped with TMR-ASO (e.g., CPD-ASO-YM155-*q*MSN), but not any other control nanoparticles, were able to induce caspase-3-activated apoptosis in HeLa cells (top gels in Figure 5e, and Figure S16, Supporting Information); no apoptosis was detected in similarly treated MCF-10A cells (bottom gels).

### 3. Conclusions

In conclusion, by using mesoporous silica nanoparticles chemically modified with a dark quencher, followed by sequential drug encapsulation, MSN capping with a dye-labeled antisense oligonucleotide and bioorthogonal surface modification with cell-penetrating poly(disulfide)s, we have successfully developed the first mesoporous silica nanoquencher characterized by high drug loading and endocytosis-independent cell uptake, and was able to quantitatively image endogenous survivin mRNA and release the loaded drug in a manner that depended on the survivin expression level in tumor cells. This novel theranostic system unifies endogenous imaging of both the target and drug release process, and on-demand drug release into a single platform. It may also be used to minimize potential cytotoxicity encountered by many existing small molecule drugs in cancer therapy. Finally, the use of *q*MSN for quantitative imaging of endogenous mRNA by taking advantage of sequence-based hybridization/de-hybridization of gated, fluorescently labeled ASO for binding/recognition of endogenous mRNA is conceptually novel, and should be universally applicable for live-cell imaging of many other biologically relevant mRNAs.

### 4. Experimental Section

**Materials:** Tetraethylorthosilicate (TEOS), *N*-cetyltrimethylammonium bromide (CTAB), 3-aminopropyltriethoxysilane (APTES), and sodium hydroxide were purchased from Sigma. YM155 was obtained from Selleckchem. Black hole quencher-2 (BHQ-2) NHS ester was purchased from Biosearch Technologies (USA).

Antibodies were purchased from following vendors: rabbit anti-cleaved caspase-3 (#9664, Cell signaling Technology), rabbit anti- $\beta$ -tubulin (#ab6064, abcam), and goat anti-rabbit IgG (#A11008, Invitrogen). Western blotting was performed by using the ECL Plus Western Kit (GE Healthcare), and imaged on an ImageQuant LAS 500 system (GE). All reagents were of analytical grades and used as received without further purification, unless otherwise indicated. All aqueous solutions were prepared by using diethyl pyrocarbonate (DEPC)-treated ultrapure water from a Milli-Q system. Phosphate buffered saline ( $10 \times 10^{-3}$  M, pH 7.4) was diluted from  $10 \times$  PBS buffer, containing  $136.7 \times 10^{-3}$  M NaCl,  $2.7 \times 10^{-3}$  M KCl,  $8.7 \times 10^{-3}$  M  $\text{Na}_2\text{HPO}_4$ , and  $1.4 \times 10^{-3}$  M  $\text{KH}_2\text{PO}_4$ . All oligonucleotides were purchased from Integrated DNA Technologies (Singapore). Their sequences are as follows:

| Probe  | RNA or DNA sequence (5'-3')                  |
|--|--|
| Synthetic survivin mRNA target                   | rArArU rUrCrA rCrArG rArArU rArGrC<br>rArCrA |
| Antisense oligo (TMR-ASO) against survivin mRNA  | TMR-TGT GCT ATT CTG TGA ATT                  |
| 18C naïve oligo (TMR-18C) as negative gatekeeper | TMR-CCC CCC CCC CCC CCC CCC                  |
| Non-complementary control synthetic target (18A) | rArArA rArArA rArArA rArArA rArArA<br>rArArA |

\*r(A/U/C/G) and (A/T/C/G) denote the corresponding ribonucleotides and deoxyribonucleotides, respectively.

Fluorescence spectra were collected on a Horiba FluoroMax-4 fluorometer. Ultraviolet-visible (UV-vis) extinction spectra were measured on a Shimadzu UV-2450 spectrophotometer. TEM images were obtained on a JEOL 2010 transmission electron microscope at an accelerating voltage of 200 kV. Zeta-potential, particle size and distribution were performed on a Malvern Nano-ZS90. Flow cytometric analysis was carried out on a BD Accuri C6 cell analyzer. The confocal cell images were obtained on a Leica TCS SP5 X Confocal microscope equipped with a 63 $\times$  water immersion objective. 3D projection of z-stack images were collected on a FV1000-X81 confocal microscope (Olympus) equipped with a water immersion objective (60 $\times$ ). HCS were acquired with an In-Cell Analyzer 2200 (GE Healthcare) equipped with a solid-state, multi-wavelength illuminator. Images were processed and quantified with In-Cell Developer Toolbox software 1.9.2. Real-time *q*PCR was carried out on a Bio-Rad MyiQ RT-PCR thermo cycler.

**Synthesis of Tz-CPD:** The Tz-CPD polymer used in this study was synthesized and characterized according to previously published procedures (Figure S1a, Supporting Information).<sup>[20a]</sup> The molecular weight of the Tz-CPD polymer was determined to be  $\approx 20$  kDa by analytical gel permeation chromatography (GPC), with an estimated stock concentration of  $\approx 200 \times 10^{-6}$  M. The  $\text{N}_3$ -RGD peptide was synthesized by standard solid-phase peptide synthesis according to previously reported procedures.<sup>[6]</sup>

**Synthesis of BHQ-2-APS,  $\text{N}_3$ -APS and Tetrazine-APS:** As shown in Figures S1b and S1c in the Supporting Information, APTES (8.6 mg) was reacted with 50  $\mu\text{L}$  of BHQ-2 NHS ester stock solution in anhydrous DMF ( $0.01 \text{ mg mL}^{-1}$ ) containing 2% diisopropylethylamine (DIPEA) overnight, as previously described.<sup>[16]</sup> Subsequently, this freshly prepared BHQ-2-APS stock was used in the next-step MSN modification without any further purifications.

For the reaction stock of  $N_3$ -APS, first, 6-azidohexanoic acid succinimidyl ester was synthesized according to published procedures as the followings.<sup>[4]</sup> 6-Bromohexanoic acid (1.50 g, 7.67 mmol) was first dissolved by stirring in anhydrous DMF (5 mL), followed by addition of sodium azide (1.0 g, 15.4 mmol) into the solution, and the mixture was stirred at 85 °C for 3 h. The mixture was diluted in dichloromethane (50 mL) and washed with hydrochloric acid (50 mL, 0.1 M). The organic layer was extracted, washed with hydrochloric acid (0.1 M), dried over anhydrous sodium sulfate, and concentrated in vacuo to yield crude 6-azidohexanoic acid (1.0 g, 83% yield) as a yellow oil-like solution. 1-Ethyl-3-(3-dimethylaminopropyl) carbodiimide (720 mg, 3.76 mmol) was added to this crude 6-azidohexanoic acid (590 mg, 3.76 mmol) dissolved in  $CHCl_3$ /DMF (9:1, 1 mL), followed by addition of *N*-hydroxysuccinimide (432 mg, 3.76 mmol). The reaction mixture was stirred at room temperature for 18 h, then diluted with  $CH_2Cl_2$  (50 mL) and washed with dilute hydrochloric acid (50 mL, 0.1 M). The organic layer was extracted, rinsed with hydrochloric acid, and washed with aqueous sodium bicarbonate and brine. The organic layer was dried over anhydrous sodium sulfate and concentrated in vacuo to yield a yellowish solution which was further purified by flash chromatography (3:7 ethyl acetate/dichloromethane) to give the pure 6-Azidohexanoic acid succinimidyl ester (600 mg, 63% yield). Characterizations of this product were in good agreement with previously reported data.<sup>[32]</sup>  $^1H$  NMR (300 MHz,  $CDCl_3$ ):  $\delta$  1.54–1.38 (m, 2H), 1.67–1.62 (m, 2H), 1.82–1.77 (q, 2H), 2.57–2.47 (q, 2H), 2.74 (br s, 4H), 3.24–3.19 (t,  $J = 6.5$  Hz, 2H). Subsequently, the reaction stock of  $N_3$ -APS was prepared by mixing 0.6  $\mu$ mol of 6-Azidohexanoic acid succinimidyl ester with APTES (8.6 mg) in anhydrous DMF (50  $\mu$ L) in the presence of 2% DIPEA overnight, and used in the next-step MSN modification without any further purifications. Tetrazine-APS was synthesized, purified, and characterized according to previous reported procedures.<sup>[6]</sup>

**Synthesis of CPD-ASO-Dox-qMSN:** As shown in Figure S2a in the Supporting Information, 3-aminopropyl-functionalized MSNs were first synthesized according to previously reported protocols.<sup>[6]</sup> Briefly, CTAB (0.1 g) was first dissolved in ultrapure water (48 mL). NaOH (2.0 M, 0.35 mL) was added to the solution and stirred for 15 min, and then the mixture was heated to 80 °C. TEOS (0.5 mL) was added dropwise into the above solution with constant stirring and APTES (0.1 mL) was added 5 min later. Upon further stirring at 80 °C for 2 h, the resulting nanoparticles were filtered, washed with methanol, and deionized (DI) water, and freeze-dried overnight. The dried 3-aminopropyl-functionalized MSNs with CTAB were used for further modification as follows. The MSNs with CTAB (1.0 mg) were dispersed in 5 mL dry toluene, followed by addition of 50  $\mu$ L (or other amounts as indicated in Figure S4 in the Supporting Information) of BHQ-2-APS and/or 50  $\mu$ L of  $N_3$ -APS. The mixture was stirred at 50 °C in a nitrogen atmosphere for 6 h. The nanoparticles were collected by centrifugation and washed with methanol and DI water, then freeze-dried overnight. The CTAB template from the obtained BHQ-MSN (*q*MSN; with or without  $N_3$  group) was subsequently removed by dispersing the nanoparticles in methanol (5 mL) containing concentrated HCl (37%, 0.3 mL). The resulting solution was stirred at room temperature for 24 h, followed by centrifugation and washing with ethanol and DI water, giving *q*MSN without CTAB. Next, TCO surface modification was done by adding to the *q*MSN (1 mg dispersed in 0.2 mL PBS) 3  $\mu$ L of  $50 \times 10^{-3}$  M TCO-PEG<sub>12</sub>-DBCO stock solution (dissolved in DMF),

and the reaction was stirred overnight, followed by centrifugation and washing with water (3 times). To load the drug (i.e., doxorubicin, or Dox), 100  $\mu$ L of the obtained TCO-*q*MSN (redispersed in  $H_2O$ , 1.0 mg  $mL^{-1}$ ) was incubated with 20  $\mu$ L of  $50 \times 10^{-3}$  M Dox stock solution (dissolved in  $H_2O$ ) for 24 h, followed by centrifugation, washed with water (2 times) and resuspension in PBS (50  $\mu$ L). The capping of the nanoparticles with ASO (or a control oligo) was next done by addition of 6.0  $\mu$ L of the oligo stock solution ( $100 \times 10^{-6}$  M), followed by incubation at 37 °C for 2 h. Upon centrifugation and washing with water (3 times), the resulting ASO-Dox-*q*MSN were redispersed in PBS (100  $\mu$ L). Finally, 5.0  $\mu$ L of the earlier-prepared Tz-CPD stock (50 M) was added to the nanoparticle solution (1.0 mg  $mL^{-1}$ , 50  $\mu$ L), and the mixture were incubated at room temperature for 1 h. Upon centrifugation and washing with water (2 times), the resulting nanoparticles were redispersed in PBS (50  $\mu$ L), giving CPD-ASO-Dox-*q*MSN (1.0 mg  $mL^{-1}$ ). CPD-ASO-*q*MSN loaded with other drugs (i.e., YM155;  $50 \times 10^{-3}$  M stock in DMSO), or no drug, were similarly prepared. Nanoparticles capped with a control oligo (i.e., TMR-18C) were similarly prepared, except TMR-18C was used in place of survivin TMR-ASO during the capping step.

**Preparation of RGD-ASO-qMSN:** The RGD-ASO-*q*MSN, used as control nanoparticles to evaluate the effect of CPD in facilitated cell uptake and improved imaging capability of *q*MSN, were prepared as the following (Figure S2b, Supporting Information). 1.0 mg of above-synthesized *q*MSN without CTAB was first suspended in 5 mL dry toluene. Tetrazine-APS (4 mg) was subsequently added and the mixture was stirred at 50 °C under a nitrogen atmosphere for 6 h. The nanoparticles were centrifuged and washed with methanol and DI water, then freeze-dried overnight to obtain Tz-*q*MSN. Upon resuspension in 0.2 mL DMF (final conc: 5 mg  $mL^{-1}$ ), the resulting solution was added 3  $\mu$ L of the TCO-PEG<sub>12</sub>-DBCO stock solution ( $50 \times 10^{-3}$  M in DMF), and the reaction was stirred overnight, followed by centrifugation and washing with DMF and DI water (2 times), then resuspension in 1.0 mL PBS to give DBCO-*q*MSN (1.0 mg  $mL^{-1}$ ). A portion of the MSN solution (50  $\mu$ L) was next added 6  $\mu$ L of the capping ASO stock solution ( $100 \times 10^{-6}$  M) and the resulting mixture was incubated at 37 °C for 2 h. Upon centrifugation, washing with water (3 times) and resuspension in 50  $\mu$ L of PBS (final MSN conc: 1.0 mg  $mL^{-1}$ ), the solution was added 5  $\mu$ L of the  $N_3$ -RGD stock solution ( $50 \times 10^{-3}$  M in  $H_2O$ ) followed by incubation at room temperature for 4 h. Upon centrifugation, washing with DI water (2 times) and resuspension in PBS (50  $\mu$ L), the resulting RGD-ASO-*q*MSN stock was obtained (1.0 mg  $mL^{-1}$ ).

**Fluorescence Quenching and Drug-Loading Efficiency of qMSN:** To determine the fluorescence quenching efficiency of ASO-*q*MSN prepared from modification with different amounts of BHQ-2-APS, 20  $\mu$ L of the TMR-ASO-capped nanoparticles (1 mg  $mL^{-1}$  in PBS) were transferred to each of two identical 1.5 mL centrifuge tubes (A and B). Tube A was added 2  $\mu$ L of synthetic survivin mRNA ( $1 \times 10^{-3}$  M; to prevent the heat-released TMR-ASO from binding back to *q*MSN surface), and the sample was heated at 95 °C for 10 min followed by dilution with 400  $\mu$ L of PBS and fluorescence measurement on a Horiba FluoroMax-4 fluorometer ( $\lambda_{ex} = 545$  nm;  $\lambda_{em} = 560$ –700 nm with max  $\lambda_{em} = 580$  nm). The resulting fluorescence reading (measured at  $\lambda_{em} = 580$  nm) from this sample was used as  $I_{full\ release}$  (100% TMR-ASO release). Tube B was directly added 400  $\mu$ L of PBS (no target and no heating) followed by fluorescence

measurement to give  $I_{\text{control}}$  (0% TMR-ASO release). The QE of  $q\text{MSN}$  was calculated as follows and shown in Figures S4a,b in the Supporting Information

$$\text{QE}\% = \frac{I_{\text{control}}}{I_{\text{full release}}} \times 100\%$$

The Dox loading efficiency was determined, as previously described,<sup>[6]</sup> by measuring the fluorescence spectra of the supernatant after loading with stock solutions containing different Dox concentrations, and comparing them with the standard calibration curve (Figure S4d, Supporting Information insert;  $\lambda_{\text{ex}} = 488 \text{ nm}$ ,  $\lambda_{\text{em}} = 558 \text{ nm}$ ). The optimized loading amount of Dox to ASO-Dox- $q\text{MSN}$  was calculated to be  $58.85 \mu\text{mol g}^{-1}$  (Figure S4d, Supporting Information). The loading efficiency of YM155 was similarly calculated to be  $72.34 \mu\text{mol g}^{-1}$ , from a standard curve obtained from YM155 stocks by measuring the UV-vis spectra ( $\lambda_{\text{abs}} = 348 \text{ nm}$ ). The amount of BHQ-2 modified on the  $q\text{MSN}$  surface was similarly determined with a standard curve generated from BHQ-2 stock solutions ( $\lambda_{\text{abs}} = 579 \text{ nm}$ ). The amount of ASO capping on the  $q\text{MSN}$  was done as previously described.<sup>[6]</sup> Briefly, by monitoring the fluorescence intensity of ASO oligos at  $580 \text{ nm}$  ( $\lambda_{\text{ex}} = 545 \text{ nm}$ ) in the supernatant and comparing it against a standard curve generated from ASO stock solutions (Figure S4c, Supporting Information), the ASO capping amount for CPD-ASO-Dox- $q\text{MSN}$  was determined to be  $18.46 \mu\text{mol g}^{-1}$ . The density of ASO oligos on the  $q\text{MSNs}$  surface was calculated as follows:  $d = c \times V/m$ , where the units of  $c$ ,  $V$ ,  $m$ , and  $d$  are in  $\text{nmol mL}^{-1}$ ,  $\text{mL}$ ,  $\text{mg}$ , and  $\text{nmol mg}^{-1}$ , respectively.

**Target Detection with Synthetic Survivin mRNA:**  $10 \mu\text{L}$  of CPD-ASO- $q\text{MSN}$  ( $1.0 \text{ mg mL}^{-1}$  in PBS) were mixed with  $85 \mu\text{L}$  of PBS containing different concentrations of synthetic Survivin mRNA or a control oligo, and the resulting mixtures were incubated at  $37^\circ\text{C}$  for 2 h and diluted with  $300 \mu\text{L}$  of PBS (giving a final volume of  $400 \mu\text{L}$  in each sample), followed by fluorescence measurements ( $\lambda_{\text{ex}} = 545 \text{ nm}$ ,  $\lambda_{\text{em}} = 580 \text{ nm}$ ). Time-dependent release experiments were similarly done ( $0.1 \text{ mg mL}^{-1}$   $q\text{MSN}$ ). Results are shown in Figure 2 in the main text.

**Target Detection with Total RNA from HeLa Cell Lysates:** HeLa cells were first seeded in 12-well dishes and incubated until 80% confluency. Upon medium removal, the cells were washed with PBS (2 times) followed by total RNA isolation using TRIzol Reagent (Invitrogen) according to manufacturer's protocols.<sup>[6]</sup> The isolated RNA was quantified (UV<sub>260/280 nm</sub> measurement) and used immediately in the following experiments. Briefly, different amounts of these total RNA isolates were added to  $10 \mu\text{L}$  of ASO- $q\text{MSN}$  ( $1.0 \text{ mg mL}^{-1}$  in PBS), and the final volume of the mixture was adjusted  $100 \mu\text{L}$  with PBS. The mixture was next incubated at  $37^\circ\text{C}$  for 2 h, followed by fluorescence measurements (Figure S5a, Supporting Information).

**Dox Controlled-Release Experiments:** Typical in vitro controlled release experiments of Dox were performed in PBS or DMEM. First, CPD-ASO-Dox- $q\text{MSN}$  were dispersed in PBS/DMEM solution to a final concentration of  $0.1 \text{ mg mL}^{-1}$ . Subsequently, different amounts of synthetic survivin mRNA (or a control oligo; in  $100 \times 10^{-6} \text{ M}$  stock) were added and the resulting mixtures were incubated at  $37^\circ\text{C}$ . Aliquots of the mixtures were taken periodically, centrifuged (at  $13,200 \text{ rpm}$ ) to collect the supernatant whose fluorescence was subsequently measured ( $\lambda_{\text{ex}} = 488 \text{ nm}$ ,

$\lambda_{\text{em}} = 558 \text{ nm}$ ). Results are shown in Figure 3 and in Figures S5b-d in the Supporting Information.

**Cell Culture:** HeLa, MCF-7, A549, A431, PC3, HepG 2, HEK 293T cell lines were cultured in DMEM cell culture medium supplemented with 10% fetal bovine serum (Hyclone) and 2% penicillin/streptomycin (PAN-Biotech) and maintained at  $37^\circ\text{C}$  in a 5%  $\text{CO}_2$  atmosphere. MCF-10A cells were cultured in mammary epithelial cell growth medium (Lonza) supplemented with  $100 \text{ ng mL}^{-1}$  cholera toxin (Sigma Aldrich), and maintained at  $37^\circ\text{C}$  in a 5%  $\text{CO}_2$  atmosphere.

**Live-Cell Imaging:** For CLSM imaging, cells were seeded in 4-well glass-bottom dishes (Greiner Bio-One) and grown until 50% confluency. After medium removal, cells were incubated with  $10 \mu\text{g mL}^{-1}$  of different  $q\text{MSNs}$  (in fresh cell medium) for different periods of incubation time. After that, cells were washed with PBS buffer twice, and then stained by Hoechst 33342 ( $V_{\text{Hoechst}}:V_{\text{DMEM}} = 1:3000$ ). The treated cells were analyzed on a Leica TCS SP5 X confocal microscope equipped with a  $63\times$  water immersion objective ( $\lambda_{\text{ex}} = 405 \text{ nm}$ ,  $\lambda_{\text{em}} = 430\text{--}460 \text{ nm}$  for Hoechst 33342;  $\lambda_{\text{ex}} = 488 \text{ nm}$ ,  $\lambda_{\text{em}} = 565\text{--}620 \text{ nm}$  for Dox and  $\lambda_{\text{ex}} = 545 \text{ nm}$ ,  $\lambda_{\text{em}} = 565\text{--}620 \text{ nm}$  for TMR). For 3D imaging, cells were seeded in 4-well glass-bottom dishes (Greiner Bio-One) and grown until 50% confluency. Upon removing medium, cells were incubated with  $10 \mu\text{g mL}^{-1}$  of the different  $q\text{MSNs}$  for different lengths of incubation time, then washed with PBS buffer (2 times) and nuclei-stained by Hoechst 33342. A FV1000-X81 confocal microscope (Olympus) equipped with a  $60\times$  water immersion objective was used to image the treated cells ( $\lambda_{\text{ex}} = 405 \text{ nm}$ ,  $\lambda_{\text{em}} = 415\text{--}475 \text{ nm}$  for Hoechst 33342;  $\lambda_{\text{ex}} = 488 \text{ nm}$ ,  $\lambda_{\text{em}} = 500\text{--}550 \text{ nm}$  for Dox, and  $\lambda_{\text{ex}} = 561 \text{ nm}$ ,  $\lambda_{\text{em}} = 580\text{--}650 \text{ nm}$  for TMR). Results are shown in Figure S8 in the Supporting Information and in the main text (Figure 4).

**High-Content Screening:** For imaging-based, HCS experiments, different cell lines were seeded in 96-well plates as previously described.<sup>[1]</sup> When cells reached 60% confluency, they were incubated with  $10 \mu\text{g mL}^{-1}$  of CPD-ASO- $q\text{MSN}$  for 4 h. Subsequently, cells were washed with PBS (2 times) and nuclei-stained by Hoechst 33342 as earlier described. Images were acquired by employing In-Cell Analyzer automated fluorescence imaging system (GE Healthcare) equipped with a  $20\times$  objective. Four images were randomly acquired from each well with a laser-based autofocus system under the same exposure conditions ( $\lambda_{\text{ex}} = 390 \pm 18 \text{ nm}$ ,  $\lambda_{\text{em}} = 432.5 \pm 48 \text{ nm}$  for Hoechst 33342;  $\lambda_{\text{ex}} = 542 \pm 27 \text{ nm}$ ,  $\lambda_{\text{em}} = 597 \pm 45 \text{ nm}$  for TMR;  $\lambda_{\text{ex}} = 542 \pm 27 \text{ nm}$  for bright-field). On average, around 300 cells were analyzed in each well. All images were subsequently processed with In-Cell Developer Toolbox software 1.9.2 by following the vendor's protocols.<sup>[20a]</sup> Both the nucleus and CPD-ASO- $q\text{MSN}$  were analyzed, and the nucleus was measured by counts while TMR fluorescence released from CPD-ASO- $q\text{MSN}$  was measured by the sum of TMR fluorescence intensity in each cell. The average intensity of released TMR fluorescence from CPD-ASO- $q\text{MSN}$  in each cell was calculated by using the sum released TMR fluorescence/Count of Hoechst. Results are shown in Figure S10 in the Supporting Information.

**Flow Cytometry:** For such experiments,  $10 \mu\text{g mL}^{-1}$  of CPD-ASO- $q\text{MSN}$  (prepared in fresh cell medium) were incubated with different cells (grown to 60% confluency) in 24-well plates at  $37^\circ\text{C}$  for 4 h. The cells were washed with cold PBS buffer (2 times) before being detached by treatment with  $200 \mu\text{L}$  of

0.25% trypsin-EDTA (ethylenediaminetetraacetic acid) at 37 °C for 2 min, then collected by centrifugation (2 min at 1000 rpm) at 4 °C. Upon further washing with 200  $\mu$ L cold PBS (2 times), the cells were resuspended in 500  $\mu$ L PBS, followed by analysis on a BD Accuri C6 cell analyzer (min. 10 000 cells were counted). Cell lines without qMSN-treatments were run concurrently as negative controls. Results are shown in Figures 4 and 5.

**Apoptosis, Cell Viability, and Western Blotting:** Cells were seeded and grown to 70–80% confluency in 12-well plates, then incubated with different qMSNs (50  $\mu$ g mL<sup>-1</sup>) at 37 °C for 24 h. Cells without treatment with qMSNs were concurrently run as negative controls. Subsequently, cells were washed with cold PBS (2 times) and detached with 0.25% trypsin-EDTA, followed by centrifugation and washing with cold PBS. Propidium iodide (PI) and Annexin V-FITC staining was next carried out by using a FITC Annexin V Apoptosis Detection Kit (BD Pharmingen, #556547) according to the manufacturer's guidelines and previously published protocols.<sup>[26a]</sup> Briefly, upon washing, cells were resuspended in 1 $\times$  binding buffer at a concentration of 1  $\times$  10<sup>6</sup> cell mL<sup>-1</sup>. 100  $\mu$ L the above cells were transferred to a 1.5 mL centrifuge tube and then co-stained with 5  $\mu$ L of FITC Annexin V and PI each, followed by addition of 400  $\mu$ L 1 $\times$  binding buffer. Subsequently, the treated cells were analyzed on a BD Accuri C6 cell analyzer (min. 10 000 cells were counted). Cell viability was performed by using XTT colorimetric cell proliferation kit (Roche) following manufacturer's guidelines and previously published protocols.<sup>[33]</sup> Briefly, HeLa cells were seeded in a 96-well plate and grown to 50–60% confluency. Cells were then treated with different qMSNs (50  $\mu$ g mL<sup>-1</sup>) in fresh DMEM medium. Cells without qMSN treatment were done concurrently as control samples. After 24 h of incubation, 50  $\mu$ L of the XTT reagent solutions were added into each well followed by incubation for another 2 h. Then proliferation absorbance of the solution was assayed by using a Bio-Rad 680 microplate reader (at 450 nm, with reference at 650 nm). Data represented the average (s.d.) of triplicates. For WB, HeLa cells were first seeded in 12-well plates and grown to 70–80% confluency, then added different qMSNs (50  $\mu$ g mL<sup>-1</sup> in DMEM medium) followed by incubation at 37 °C for 24 h. Cells without any treatment were used as negative controls. The cells were next washed with cold PBS (3 times), collected and the resulting cell pellets were lysed in the Laemmli buffer (62.5  $\times$  10<sup>-3</sup> M Tris-HCl, pH 6.8, 20% glycerol, 2% SDS, 2  $\times$  10<sup>-3</sup> M DTT, Halt phosphatase inhibitor and Roche proteinase inhibitor cocktail) by boiling at 95 °C for 10 min. Protein concentration was determined by using the Bradford Protein Assay (Bio-Rad, #162-0177) as previously described.<sup>[2]</sup> Subsequently, WB analysis was performed by using the appropriate primary and secondary antibodies according to previously reported protocols.<sup>[6]</sup>

**Downregulation and qPCR:** For YM155-induced downregulation experiment of survivin mRNA in HeLa cells, the cells were first seeded in 24-well plates for 12 h, then incubated with different amounts of a YM155 stock solution (100  $\times$  10<sup>-6</sup> M in DMSO) at 37 °C for 48 h. The intracellular expression levels of survivin mRNA were determined by real-time quantitative PCR (qPCR) analysis. Next, cells (at 80% confluency) were incubated with different qMSNs (50  $\mu$ g mL<sup>-1</sup>) at 37 °C for 24 h. Upon medium removal, RNA isolation was performed using TRIzol Reagent (Invitrogen) following the manufacturer's protocols. The concentration of total RNA was determined and adjusted to 10 ng  $\mu$ L<sup>-1</sup> by using a Nanodrop spectrometer (UV<sub>260/280 nm</sub>). Next, a TaqMan High-Capacity cDNA

Reverse Transcription Kit (Applied Biosystems) was used to reverse transcribe RNA to cDNA (25 °C, 10 min; 37 °C, 120 min; 85 °C, 5 min; 4 °C,  $\infty$ ). The qPCR was conducted with a TaqMan Universal Master Mix II (no UNG) on a Bio-Rad MyiQ RT-PCR thermo cycler (95 °C, 10 min; followed by 40 cycles of 95 °C, 15 s; 60 °C, 60 s). The corresponding primers used in this experiment were purchased from Life Technologies (Hs04194392\_s1, control primers: Hs03929097\_g1). The relative expression of survivin mRNA was quantified by normalization against an endogenous control of GAPDH mRNA by using the 2<sup>- $\Delta$ CT</sup> method,<sup>[6]</sup> in which  $\Delta$ CT = CT<sub>survivin</sub> - CT<sub>GAPDH</sub>. All qPCR reactions were performed in triplicate. Results are shown in Figures S9, S10, and S14 in the Supporting Information.

## Supporting Information

Supporting Information is available from the Wiley Online Library or from the author.

## Acknowledgements

Funding was provided by National Medical Research Council (CBRG/0038/2013), Ministry of Education (MOE2013-T2-1-048) of the Singapore government and Natural Science Foundation of China (51403065, sklssm201730). The authors thank Yan Tong (NUS) for assistance with 3D images, and Prof. Yong Zhang (NUS) for use of Nano-ZS90 instrument.

## Conflict of Interest

The authors declare no conflict of interest.

- [1] a) K. T. Nguyen, Y. L. Zhao, *Acc. Chem. Res.* **2015**, *48*, 3016; b) H. Dong, J. Lei, L. Ding, Y. Wen, H. Ju, X. Zhang, *Chem. Rev.* **2013**, *113*, 6207.
- [2] a) Z. Li, J. C. Barnes, A. Bosoy, J. F. Stoddart, J. I. Zink, *Chem. Soc. Rev.* **2012**, *41*, 2590; b) R. M. Graybill, R. C. Bailey, *Anal. Chem.* **2016**, *88*, 431; c) C. Coll, A. Bernardos, R. Martinez-Manez, F. Sancenon, *Acc. Chem. Res.* **2013**, *46*, 339.
- [3] a) S. Pan, H. Zhang, C. Wang, S. C. L. Yao, S. Q. Yao, *Nat. Prod. Rep.* **2016**, *33*, 612; b) G. C. Terstappen, C. Schlupen, R. Raggiaschi, G. Gaviraghi, *Nat. Rev. Drug Discovery* **2007**, *6*, 891; c) B. J. Leslie, P. J. Hergenrother, *Chem. Soc. Rev.* **2008**, *37*, 1347.
- [4] a) E. Aznar, M. Oroval, L. Pascual, J. R. Murgu, R. Martinez-Manez, F. Sancenon, *Chem. Rev.* **2016**, *116*, 561; b) N. Song, Y.-W. Yang, *Chem. Soc. Rev.* **2015**, *44*, 3474.
- [5] a) C.-H. Lu, I. Willner, *Angew. Chem. Int. Ed.* **2015**, *54*, 12212; b) P. Zhang, F. Cheng, R. Zhou, J. Cao, J. Li, C. Burda, Q. Min, J. Zhu, *Angew. Chem. Int. Ed.* **2014**, *53*, 2371; c) E. Climent, R. Martinez-Manez, F. Sancenon, M. D. Marcos, J. Soto, A. Maquieira, P. Amoros, *Angew. Chem. Int. Ed.* **2010**, *49*, 7281; d) C. Chen, J. Geng, F. Pu, X. Yang, J. Ren, X. Qu, *Angew. Chem. Int. Ed.* **2011**, *50*, 882.
- [6] C. Yu, L. Qian, M. Uttamchandani, L. Li, S. Q. Yao, *Angew. Chem. Int. Ed.* **2015**, *54*, 10574.

- [7] a) T. Xia, M. Kovochich, M. Liong, H. Meng, S. Kabehie, S. George, J. I. Zink, A. E. Nel, *ACS Nano* **2009**, *3*, 3273; b) S. B. Hartono, W. Gu, F. Kleitz, J. Liu, L. He, A. P. J. Middelberg, C. Yu, G. Q. Lu, S. Z. Qiao, *ACS Nano* **2012**, *6*, 2104; c) J. L. Townson, Y. Lin, J. O. Agola, E. C. Carnes, H. S. Leong, J. D. Lewis, C. L. Haynes, C. J. Brinker, *J. Am. Chem. Soc.* **2013**, *135*, 16030.
- [8] X.-L. Li, N. Hao, H.-Y. Chen, J.-J. Xu, *Anal. Chem.* **2014**, *86*, 10239.
- [9] a) H. Xing, N. Y. Wong, Y. Xiang, Y. Lu, *Curr. Opin. Chem. Biol.* **2012**, *16*, 429; b) F. Hovelmann, O. Seitz, *Acc. Chem. Res.* **2016**, *49*, 714.
- [10] a) J. I. Cutler, E. Auyeung, C. A. Mirkin, *J. Am. Chem. Soc.* **2011**, *134*, 1376; b) N. Li, H. Yang, W. Pan, W. Diao, B. Tang, *Chem. Commun.* **2014**, *50*, 7473; c) Y. Yang, J. Huang, X. Yang, K. Quan, H. Wang, L. Ying, N. Xie, M. Ou, K. Wang, *J. Am. Chem. Soc.* **2015**, *137*, 8340.
- [11] J. S. Sun, Y. L. Xianyu, X. Y. Jiang, *Chem. Soc. Rev.* **2014**, *43*, 6239.
- [12] a) A. Jayagopal, K. C. Halfpenny, J. W. Petez, D. W. Wright, *J. Am. Chem. Soc.* **2010**, *132*, 9789; b) N. Li, C. Chang, W. Pan, B. Tang, *Angew. Chem. Int. Ed.* **2012**, *51*, 7426.
- [13] a) Z. Wu, G.-Q. Liu, X.-L. Yang, J.-H. Jiang, *J. Am. Chem. Soc.* **2015**, *137*, 6829; b) I. M. Pedersen, G. Chug, S. Wieland, S. Volinia, C. M. Croce, F. V. Chisari, M. David, *Nature* **2007**, *449*, 919.
- [14] Li et al. in reference 12b reported a molecular beacon (MB)-coated AuNP for mRNA imaging with Dox intercalated in the stem region of MB. Such system was able to deliver Dox to cells but had a very low drug loading efficiency and could not work with most other drugs.
- [15] A. R. Buxbaum, G. Haimovich, R. H. Singer, *Nat. Rev. Mol. Cell Biol.* **2015**, *16*, 95.
- [16] a) X. Huang, M. Swierczewska, K. Y. Choi, L. Zhu, A. Bhirde, J. Park, K. Kim, J. Xie, G. Niu, K. C. Lee, S. Lee, X. Chen, *Angew. Chem. Int. Ed.* **2012**, *51*, 125; b) R. Qian, L. Ding, H. Ju, *J. Am. Chem. Soc.* **2013**, *137*, 13282.
- [17] a) J. Krützfeldt, N. Rajewsky, R. Braich, K. G. Rajeev, T. Tuschl, M. Manoharan, M. Stoffel, *Nature* **2005**, *438*, 685; b) J. Li, S. Tan, R. Kooger, C. Zhang, Y. Zhang, *Chem. Soc. Rev.* **2014**, *43*, 506.
- [18] Y. Chi, X. Wang, Y. Yang, C. Zhang, H. C. Ertl, D. Zhou, *Mol. Ther. Nucleic Acids* **2014**, *3*, e208.
- [19] a) N. K. Devaraj, R. Weissleder, *Acc. Chem. Res.* **2011**, *44*, 816; b) E. M. Sletten, C. R. Bertozzi, *Acc. Chem. Res.* **2011**, *44*, 666.
- [20] a) J. Fu, C. Yu, L. Li, S. Q. Yao, *J. Am. Chem. Soc.* **2015**, *137*, 12153; b) G. Gasparini, E.-K. Bang, G. Molinard, D. V. Tulumello, S. Ward, S. O. Kelley, A. Roux, N. Sakai, S. Matile, *J. Am. Chem. Soc.* **2014**, *136*, 6069; c) E.-K. Bang, G. Gasparini, G. Molinard, A. Roux, N. Sakai, S. Matile, *J. Am. Chem. Soc.* **2013**, *135*, 2088.
- [21] C. Yu, L. Qian, J. Ge, J. Fu, P. Yuan, S. C. L. Yao, S. Q. Yao, *Angew. Chem. Int. Ed.* **2016**, *55*, 9272.
- [22] S. Ziegler, V. Pries, C. Hedberg, H. Waldmann, *Angew. Chem. Int. Ed.* **2013**, *52*, 2744.
- [23] P.-Y. Yang, K. Liu, M. H. Ngai, M. J. Lear, M. Wenk, S. Q. Yao, *J. Am. Chem. Soc.* **2010**, *132*, 656.
- [24] H. Shi, C. Zhang, G. Y. J. Chen, S. Q. Yao, *J. Am. Chem. Soc.* **2012**, *134*, 3001.
- [25] Z. Li, L. Li, P. Hao, C. Y. J. Tan, X. Cheng, G. Y. J. Chen, S. K. Sze, H.-M. Shen, S. Q. Yao, *Angew. Chem. Int. Ed.* **2013**, *52*, 8551.
- [26] Z. Li, D. Wang, L. Li, S. Pan, Z. Na, C. Y. J. Tan, S. Q. Yao, *J. Am. Chem. Soc.* **2014**, *136*, 9990.
- [27] Y. Su, S. Pan, Z. Li, L. Li, X. Wu, P. Hao, S. K. Sze, S. Q. Yao, *Sci. Rep.* **2015**, *5*, 7724.
- [28] a) B. R. Lannine, L. R. Whitby, M. M. Dix, J. Douhan, A. M. Gilbert, E. C. Hett, T. Johnson, C. Joslyn, J. C. Kath, S. Niessen, L. R. Roberts, M. E. Schnute, C. Wang, J. J. Hulce, B. X. Wei, L. O. Whiteley, M. M. Hayward, B. F. Cravatt, *Nat. Chem. Biol.* **2014**, *10*, 760; b) G. M. Simon, M. J. Niphakis, B. F. Cravatt, *Nat. Chem. Biol.* **2013**, *9*, 200.
- [29] a) J. Park, S. Oh, S. B. Park, *Angew. Chem. Int. Ed.* **2012**, *51*, 5447; b) Y. Futamura, M. Muroi, H. Osada, *Mol. Biosyst.* **2013**, *9*, 897.
- [30] a) K. Yamanaka, T. Nakahara, T. Yamauchi, A. Kita, M. Tekeuchi, F. Kiyonaga, N. Kaneko, M. Sasamata, *Clin. Cancer Res.* **2011**, *17*, 5423; b) T. Nakahara, A. Kita, K. Yamanaka, M. Mori, N. Amino, M. Takeuchi, F. Tominaga, I. Kinoyama, A. Matsuhisa, M. Kudou, M. Sasamata, *Cancer Sci.* **2011**, *102*, 614.
- [31] G. E. Winter, B. Radic, C. Mayor-Ruiz, V. A. Blomen, C. Trefzer, R. K. Kandasamy, K. V. M. Huber, M. Gridling, D. Chen, T. Klampfl, R. Kralovics, S. Kubicek, O. Fernandez-Capetillo, T. R. Brummelkamp, G. Superti-Furga, *Nat. Chem. Biol.* **2014**, *10*, 768.
- [32] C. Grandjean, A. Boutonnier, C. Guerreiro, J. M. Fournier, L. A. Mulard, *J. Org. Chem.* **2005**, *70*, 7123.
- [33] a) Z. Na, S. Pan, M. Uttamchandani, S. Q. Yao, *Angew. Chem. Int. Ed.* **2014**, *53*, 8421; b) H. Wu, J. Ge, S. Q. Yao, *Angew. Chem. Int. Ed.* **2010**, *49*, 6528.

Received: February 20, 2017  
Revised: March 17, 2017  
Published online: